Photodiagnosis and Photodynamic Therapy 34 (2021) 102286

Contents lists available at ScienceDirect

Photodiagnosis and Photodynamic Therapy

journal homepage: www.elsevier.com/locate/pdpdt

Robust antimicrobial photodynamic therapy with curcumin-poly (lactic-co-glycolic acid) nanoparticles against COVID-19: A preliminary *in vitro* study in Vero cell line as a model

Maryam Pourhajibagher [a], Maryam Azimi [b,c], Vahid Haddadi-Asl [d], Hanie Ahmadi [d], Mehrdad Gholamzad [e], Sara Ghorbanpour [f], Abbas Bahador [f,g,*]

[a] *Dental Research Center, Dentistry Research Institute, Tehran University of Medical Sciences, Tehran, Iran*
[b] *Immunology Research Center, Institute of Immunology and Infectious Diseases, Iran University of Medical Sciences (IUMS), Tehran, Iran*
[c] *Department of Immunology, School of Medicine, Tehran University of Medical Sciences, Tehran, Iran*
[d] *Department of Polymer Engineering and Color Technology, Amirkabir University of Technology, Tehran, Iran*
[e] *Department of Microbiology and Immunology, Faculty of Medicine, Tehran Medical Sciences, Islamic Azad University, Tehran, Iran*
[f] *Department of Medical Microbiology, School of Medicine, Tehran University of Medical Sciences, Tehran, Iran*
[g] *Fellowship in Clinical Laboratory Sciences, Iran University of Medical Sciences, Tehran, Iran*

ARTICLE INFO

Keywords:
Antimicrobial photodynamic therapy
Coronavirus
COVID-19
Curcumin
PLGA
SARS-CoV-2

ABSTRACT

Background: In this study, the ability of antimicrobial photodynamic therapy (aPDT) as a treatment approach and adjuvant therapy using curcumin-poly (lactic-co-glycolic acid) nanoparticles (Cur@PLGA-NPs) to inactivate Coronavirus disease 2019 (COVID-19) in plasma was investigated. Furthermore, to verify whether the quality requirement of aPDT-treated plasma is acceptable, the differences of the levels of clotting factors, total plasma proteins, and anti-A and/or anti-B antibodies titrations in plasma of patient before and after aPDT treatment were investigated.

Materials and Methods: Cur@PLGA-NPs was synthesized using Electrospinning process and characterized by different analysis including Scanning Electron Microscope (SEM), Transmission Electron Microscope (TEM), and Fourier Transform Infrared (FTIR) spectroscopy assays. The presence of the SARS-CoV-2 in the plasma samples of patients suspected of having COVID-19 was confirmed by real-time reverse transcription-polymerase chain reaction (RT-PCR) assay. Then, the treated plasma samples with Cur@PLGA-NPs plus blue laser were exposed to Vero cells. Eventually, cell cytotoxicity and apoptotic effects of treated Vero cells were evaluated. Levels of clotting factors including prothrombin time (PT) and activated partial thromboplastin time (APTT), total plasma proteins, and anti-A and/or anti-B antibodies measurements were performed using the coagulometer, method of Bradford, and titration procedure, respectively.

Results: The presence of SARS-CoV-2 was positive in 84.3 % of samples. Different concentrations of Cur@PLGA-NPs (3, 5, 7, and 10 % wt.), the irradiation times of blue laser (1, 3, and 5 min), and aPDT with the maximum dosed of blue laser light (522.8 J/cm^2) plus 10 % wt. Cur@PLGA-NPs had no cytotoxicity. Although there were significant cell degradation and apoptotic effects in treated Vero cells with treated plasma using 10 % wt. Cur@PLGA-NPs, and a blue laser at an energy density of 522.8 J/cm^2, no visible changes in cells and apoptosis were observed following aPDT. Total plasma protein content, PT, APTT, and anti-A and/or anti-B antibodies titers showed no significant changes ($P > 0.05$ for all comparisons) in treated plasma as compared to untreated plasma.

Conclusion: aPDT exhibited *in vitro* anti-COVID-19 activities in the treated plasma containing SARS-COV-2 without Vero cell apoptosis and any adverse effects on plasma quality in aPDT-exposed plasma.

* Corresponding author at: Department of Medical Microbiology, School of Medicine, Tehran University of Medical Sciences, Tehran, Iran.
E-mail address: abahador@sina.tums.ac.ir (A. Bahador).

https://doi.org/10.1016/j.pdpdt.2021.102286
Received 16 November 2020; Received in revised form 23 March 2021; Accepted 2 April 2021
Available online 7 April 2021

1. Introduction

Coronavirus disease 2019 (COVID-19) is a contagious respiratory illness caused by a new strain of coronavirus named Severe Acute Respiratory Syndrome Coronavirus-2 (SARS-CoV-2). The first case of COVID-19 was identified in Wuhan, Hubei province, China, in December 2019. It has since rapidly spread worldwide, resulting in an ongoing pandemic [1]. SARS-CoV-2 is an enveloped virus with a positive sense, single-stranded RNA genome [2]. It can enter the host cells by the transmembrane spike (S) glycoprotein. This glycoprotein contains a receptor-binding domain (RBD) that specifically recognizes its host receptor angiotensin-converting enzyme 2 (ACE2). By inhibiting RBD binding to its receptor can be prevented from the entry of the SARS-CoV-2 to the host cells and reduced the proliferation and pathogenicity of the virus [3]. SARS-CoV-2 is able to invade and affect the upper respiratory tract (throat, nose, and sinuses) and the lower respiratory tract (lungs). The lungs are the main organ affected by SARS-CoV-2 because the virus accesses type II alveolar cells of the lungs *via* ACE2, which is most abundant in these pneumocytes. As the alveolar disease progresses, SARS-CoV-2 may also enter the bloodstream from the lungs, and systemic disease might develop as well as death may follow [3].

According to the literature, there are few antiviral drugs for the treatment of COVID-19. Primary and secondary bio-molecules have recently been introduced for optical and electrical diagnosis as well as monitoring of SARS-CoV-2 infections using the spectroscopy, fluorescence, and conductivity-based techniques [4].

It has been revealed that human airway epithelial cells highly express the receptors for SARS-CoV-2, including transmembrane serine proteinase 2 (TMPRSS2) and angiotensin-converting enzyme 2 (ACE2), but they are expensive and do not proliferate indefinitely. However, some infinitely proliferating cell lines, including Calu-3, Caco-2, Huh7, and HEK293 T have been used in SARS-CoV-2 infection experiments. These cell lines generate low titer of infectious SARS-CoV-2 and do not exactly mimic human physiological systems and complexity. Regarding this limitation, valuable information about infection and replication of SARS-CoV-2 can be learned from studies using these cell lines. Among the several infinitely proliferating cell lines, a cell line, such as Vero cells, that can easily replicate and isolate higher titer virus is essential for efficient SARS-CoV-2 infection experiments. Despite the primary human airway epithelial cells, Vero cells do not produce interferon (IFN) when infected with viruses including SARS-CoV-2. The IFN deficiency permits SARSCoV-2 to replicate efficiently in Vero cells and has given a high titer of the virus [5].

Antimicrobial photodynamic therapy (aPDT) as a treatment modality is widely used to inactivate/reduce the microbial population [6,7]. The reports are available on the application of aPDT to combat viral infections [8–10]. aPDT involves the use of a non-toxic dye named photosensitizer and visible light of a specific wavelength in the presence of oxygen to produce the reactive photoproducts including reactive oxygen species (ROS) that can cause fundamental damage to viral structures which are involved in causing infection. [8,10–14].

Curcumin (Cur) is a natural polyphenol derived from the turmeric rhizomes (*Curcuma longa* L.) which have been reported to have a wide range of pharmacological effects including antiviral activity [15]. It has been demonstrated that the antimicrobial effects of Cur are potentiated by the presence of light (430–450 nm), and the phototoxicity is related to the generation of ROS. Unfortunately, Cur evidences different problems for its clinical application, including extremely poor oral bioavailability, low-aqueous solubility, inadequate tissue absorption, and rapid systemic clearance [16]. To overcome these drawbacks, different delivery systems and strategies such as nano-encapsulation of Cur in poly (lactic-co-glycolic acid) (PLGA) have been investigated [17, 18]. PLGA, a copolymer of polylactic acid and polyglycolic acid, has been approved by the US Food and Drug Administration for biomedical and pharmaceutical applications [17].

Many studies have been done on PLGA as a drug carrier [18–21]. One of the drug delivery methods that has attracted the attention of researchers in recent years is the electrospray method. This method promises to encapsulate the drug effectively and allowing for excellent control of the microsphere architecture [18]. The polyphenol Cur is applied in many critical conditions such as inflammatory and oxidative conditions, metabolic syndrome, anxiety, *etc.* [20].

Recently, several clinical trials describe the use of aPDT as an adjuvant therapy which is defined as additional treatment given after the primary/ main treatment against viral infections, to make the primary treatment more likely to be successful. [22–24]. Many reports have also emerged over the years of the use of aPDT as an effective methodology for sterilization of blood or blood products [28–31].

Plasma contains important components including dissolved proteins (*e.g.*, albumins, and globulins), and clotting factors. Plasma quality is currently assessed *in vitro*, using coagulation assays, measurements of total protein, and determination of levels of blood group antibodies (A and B) [28–30]. One-stage coagulation tests including prothrombin time (PT) and activated partial thromboplastin time (APTT) are the most widely used tests to investigate coagulation disorders. The PT test is used to monitor specifically the quantity and quality of the plasma coagulation factors VII, V, and X, fibrinogen, and prothrombin. A prolonged PT reveals a decrease in the quantity and quality of the mentioned factors. The activated partial APTT is a test performed to investigate bleeding abnormalities specifically the missing or defective of the intrinsic (Factors XII, XI, VIII, IX) and common clotting pathways [28]. The importance of the measurement anti-A and anti-B is hemagglutinins in the serum originates from the universality of its antibodies. It has been revealed that the levels of anti-A and/or anti-B antibodies appear to be influenced mainly by interfering factors and determination of their levels (titers) and reactivity are the main indicator of plasma quality [29]. The content of total plasma proteins is another main indicator mentioned in the quality requirement of plasma. In order to fully understand the quality of treated plasma, it should be evaluated the content of total plasma proteins [29].

Nevertheless, no research has yet been reported to show the effects of aPDT on SARS-CoV-2 using Cur@PLGA-NPs. This study aimed to evaluate the photoelimination effects of Cur@PLGA-NPs plus blue laser light against the plasma samples containing SARS-CoV-2 in Vero cells. Furthermore, to verify whether the quality requirement of aPDT-treated plasma is suitable, the current study was conducted to investigate the differences of the levels of clotting factors, total plasma proteins, and anti-A and/or anti-B antibodies titrations in plasma of patient before and after aPDT treatment.

2. Materials and methods

2.1. Patient selection

This study was approved by the Ethics Commission of Tehran University of Medical Sciences, Tehran, Iran under protocol IR.TUMS.VCR.REC.1399.490. The study was outlined to the patients and all of them provided informed consent. The blood samples were collected from the patients suspected of having COVID-19 referred to Bouali Hospital, Islamic Azad University (BHIAU), Tehran, Iran following inclusion criteria: demographic data, medical history, exposure history, symptoms, signs, and chest computed tomographic (CT) scans. The presence of SARS-CoV-2 was then confirmed by real-time reverse transcription-polymerase chain reaction (RT-PCR) assay.

2.2. Plasma products

After collecting the blood samples into vacutainer tubes containing ~1.8 mg K_2EDTA per mL blood, the tubes were inverted carefully 10 times to mix blood and anticoagulant. Then, the samples were immediately centrifuged at 1000–2000 RCF at room temperature for 10 min.

After centrifugation, the plasma was visible at the upper part of the blood sample.

2.3. Detection of SARS-CoV-2 and determine the load of the virus by RT-PCR assay

After collecting the plasma samples, RT-PCR assay was done to confirm the presence of SARS-CoV-2. The RNAs were extracted through the Trizol method from the plasma specimens. RNase-free DNase I treatment kit and a Revert Aid First-Strand cDNA Synthesis kit (both Thermo Fisher Scientific, Waltham, MA, USA) were used according to the manufacturer's protocol for the elimination of genomic DNAs from extracted RNA sample and synthesis of the first-strand cDNA, respectively. Open reading frame 1ab (ORF1ab) was tested during the RT-PCR assay. The primers *ORF1ab* -forward (5′−CCCTGTGGGTTTTACACTTAA -3′), *ORF1ab* -reverse (5′-ACGATTGTGCATCAGCTGA-3′) were designed using Primer3 v. 4.0 (http://frodo.wi.mit.edu/primer3/). All reactions were performed on the Roche Light cycler® 96 Real-Time PCR under the following conditions: incubation at 50 °C for 15 min and 95 °C for 5 min, 40 cycles of denaturation at 94 °C for 15 s, and extending at 55 °C for 45 s. According to the National Institute for Viral Disease Control and Prevention (China) (http://ivdc.chinacdc.cn/kyjz/202001/t20200121_211337.html), a cycle threshold value (Ct-value), less than 37 was defined as a positive test result, and a Ct-value of 40 or more was defined as a negative test, required confirmation by retesting.

2.4. Included patients

Of the 32 patients suspected of having COVID-19 who hospitalized to BHIAU between July and August 2020, 27 patients were eventually diagnosed with the COVID-19 using SARS-CoV-2 RT-PCR and included in the current study.

2.5. Synthesis of Cur@PLGA-NPs as a photosensitizer

According to our previous study, Cur@PLGA-NPs was synthesized by the Electrospraying method [21]. Briefly, the mixture of dimethylformamide (DMF; Merck, Darmstadt, Germany) and chloroform (Merck, Darmstadt, Germany) with a volume ratio of 1–3 was selected as the solvent system. PLGA (with an inherent viscosity midpoint of 2.3 dL/g; Purac corporation) was added to the solvent system to increase its concentration by 0.5 %w/w. After that, 2 mM Cur (Sigma-Aldrich, Steinheim, Germany) was poured into the viscous solution, and the mixing process continued for 24 h. After the homogenous solution was obtained, the electrospinning process for the preparation of nanoparticles began, as follows: 5 mL of the resulting solution was poured into a syringe equipped with a 22-gauge needle. The distance from the needle to the collector was set at 20 cm. Then, a voltage of 20 kV was applied to form nanoparticles on the collector, which was covered with aluminum foil. The flow rate was fixed on 2 mL/h, which is low enough to allow the solvent to evaporate completely, preventing secondary droplets. The process was performed at room temperature and the foil was placed in a vacuum dryer to remove any remaining solvent from the particles. Finally, the nanoparticles were extracted from the mentioned foil. The schematic diagram of Cur@PLGA-NLs synthesis is shown in Fig. 1.

2.6. Characterization of the core-shell Cur@PLGA-NPs

Morphology and particle size distribution were studied by the Scanning Electron Microscope (SEM; SERON AIS-2100, South Korea) analysis, the accelerating voltage was 15 kV. Particle size distribution was evaluated by ImageJ (image analyzer software developed by the National Institute of Health, USA). To further examine the morphology and core-shell structure of the nanoparticles, the Transmission Electron Microscope (TEM; Zeiss EM10C) test with an accelerating voltage of 80 Kv, was performed. In addition, to investigate possible interactions between components, Fourier Transform Infrared (FTIR) spectroscopy analysis (Bomem, Canada) in a range of 400-4000 cm^{-1} was done.

2.7. Absorption spectra of Cur@PLGA-NPs

The absorption spectra of synthesized Cur@PLGA-NPs was carried out by UV–vis spectrophotometer, scanning the absorbance spectra in the range of 300–600 nm wavelength.

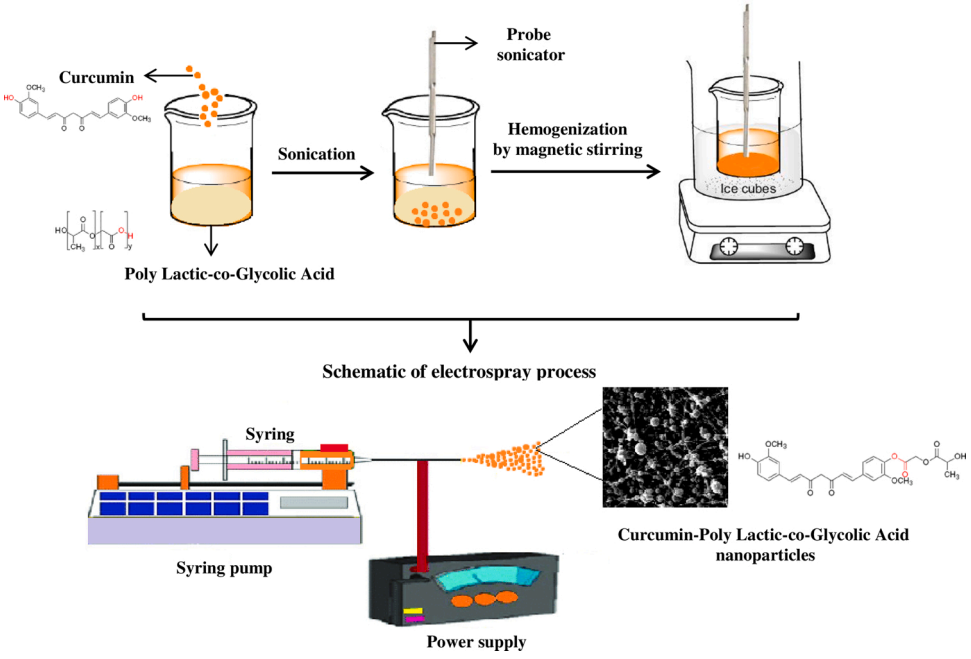

Fig. 1. The schematic diagram of Cur@PLGA-NLs synthesis.

2.8. Evaluation of drug loaded efficiency

The percentage of Cur incorporated was determined by centrifuging the Cur@PLGA-NPs at 9000 rpm at room temperature for 30 min. The supernatant was then obtained to measure the absorbance at 425 nm using an UV–vis spectrophotometer. The encapsulation efficiency (EE) and the Cur loading capacity (LC) were determined using the following equations:

$$EE\% = \frac{\text{total amount of Cur} - \text{free Cur}}{\text{total amount of Cur}} \times 100$$

$$LC\% = \frac{\text{total amount of Cur} - \text{free Cur}}{\text{nanoparticles weight}} \times 100$$

2.9. Physical stability of Cur@PLGA-NPs

To evaluate shelf life, Cur@PLGA-NPs was stored in the containers at 4 °C and 37 °C. According to the previous study [32], the particle size, polydispersity index, and zeta potential were assessed at different time intervals during storage for 30 days.

2.10. Preparation of Vero cell line culture

Normal African Green Monkey Kidney Epithelial Cells (Vero cell line; IBRC C10001) purchased from the Iranian Biological Resource Center (Tehran, Iran) was cultured in the Dulbecco's Modified Eagle Medium (DMEM) supplemented with 2 mM L-glutamine, 10 % fetal bovine serum (FBS), 100 µg/mL amphotericin B and 1% penicillin/streptomycin antibiotic solution (all purchased from Sigma-Aldrich, Steinheim, Germany) and maintained in a humidified incubator at 37 °C with a 95 % air and 5% CO_2 atmosphere. The medium was changed every 3–4 days.

2.11. Light source

A continuous blue laser (Laser Diode Stabilizer LDS201, Asha beam profile Co., Iran; Fig. 2) at the wavelength of 450 ± 10 nm with an output intensity of 1.6 W/cm^2 was used as a light source. The output power at the optic tip was measured by a photodiode power meter (PMB-104 power meter, Asha beam profile Co., Iran).

2.12. Experimental design

2.12.1. Treatment of the plasma containing SARS-CoV-2 with a photosensitizer, blue laser light, and aPDT

While the viral load is different in the Plasma of the patients with COVID-19, to correctly interpret the results of the current study, the viral load in the plasma samples of all patients was adjusted to the minimal viral load in plasma samples among patient by adding sterile plasma. 150 µL of plasma containing SARS-CoV-2 were added to the wells of a 96-well flat-bottom microtiter plate (JET BIOFIL®, Jet Bio-Filtration Co., Ltd, Guangzhou, China). Then, 150 µL of Cur@PLGA-NPs with different concentrations (3, 5, 7, 10, and 15 % wt.) were added to the wells in column one. In column two, the plasma was irradiated with a blue laser for 1, 3, and 5 min under the single wavelength of 450 ± 10 nm with energy densities of 104.5, 313.7, and 522.8 J/cm^2, respectively. In the next columns, aPDT was performed so that after 5 min of adding the non-cytotoxic highest concentration of Cur@PLGA-NPs to the plasma, the cells were exposed to the highest energy density of the blue laser light. All experiments were performed under the class III biological safety cabinet.

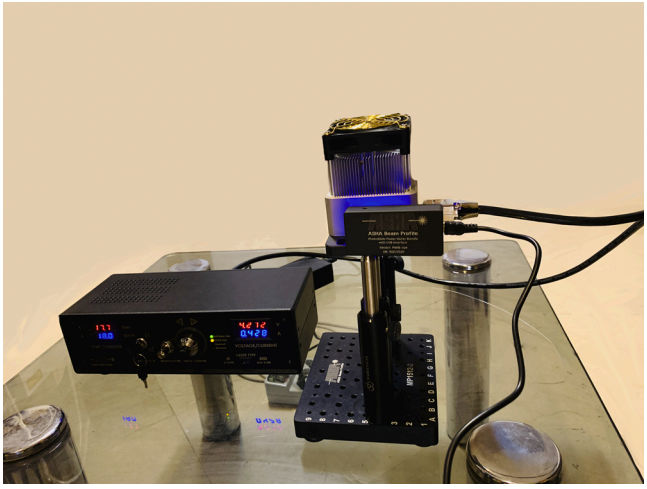

Fig. 2. The blue laser device used in this study.

2.12.2. Treatment of the Vero cell lines with a photosensitizer, blue laser light, and aPDT

Similar to the above section, Vero cell lines were treated with a photosensitizer, blue laser light, and aPDT. Briefly, in the third subculture of Vero cells, a seeding density of 1.0 × 10^5 cells/well was placed in a flat-bottomed 96-well cell culture microplate and allowed to adhere for 24 h at 37 °C in a CO_2 incubator. After 24 h of incubation, Vero cells were then treated with different concentrations of Cur@PLGA-NPs, different times of blue laser light irradiation, and aPDT with the non-cytotoxic highest concentration of Cur@PLGA-NPs plus the highest energy density of the blue laser light. After 24 h incubation at 37 °C in a CO_2 incubator, the cells were washed with sterile phosphate-buffered saline (PBS) to eliminate non-adherent cells. Finally, a 3-(4,5dimethylthiazol-2-yl)-2,5-diphenyltetrazolium bromide (MTT) cell proliferation assay kit (Sigma-Aldrich, Steinheim, Germany) was used based on the manufacturer's instructions to evaluate the cell cytotoxicity using a microplate reader (Bio-Tek Instruments, USA) at 540 nm.

2.13. Cell cytotoxicity assessment of treated Vero cell lines with treated plasma containing SARS-CoV-2

About 1.0 × 10^5 cells/well were seeded to a flat-bottom 96-well microtiter plate and incubated at 37 °C in a CO_2 incubator for 24 h. After the Vero cells grew into a single layer in a 96-well microtiter plate, the culture medium was discarded and the treated plasma with the non-cytotoxic highest concentration of Cur@PLGA-NPs (10 % wt.) and the highest energy density of the blue laser light (522.8 J/cm^2) was added. After 24 h, the cell cytotoxicity of treated Vero cell lines was determined using the MTT cell proliferation assay kit at 540 nm.

2.14. Estimation of the apoptotic effects in treated Vero cell lines with treated plasma containing SARS-CoV-2

To estimate the apoptotic effects of treated plasma containing SARS-CoV-2 on Vero cells, about 1.0 × 10^5 cells/well were seeded to a flat-bottom 96-well microtiter plate and 150 µL of the treated plasma was added and incubated at 37 °C in a CO_2 incubator for 24 h. The cells were then washed with PBS and divided into two equal parts for flow cytometry and fluorescent staining as follows:

2.14.1. Detection of apoptosis by flow cytometry

The washed cells were re-suspended in 100 µL 1x Annexin V-FITC binding buffer. Then, 5 µL Annexin V-FITC and 5 µL propidium iodide (PI) were added to each well and incubated at room temperature in dark for 15 min. All process was carried out according to the manufacturer's instructions (BD Biosciences, San Diego, CA, USA). Finally, the percent of apoptotic cells was determined by flow cytometry and data were analyzed using ver-7 Flowjo software.

2.14.2. Detection of apoptosis by fluorescent staining

Paraformaldehyde solution (4% in PBS) was added to fix the washed cells at room temperature for 30 min. The cells were then washed with PBS (pH 7.2) and stained with dual acridine orange (AO) /ethidium bromide (EB) fluorescent staining solution (100 μg/mL AO and 100 μg/mL EB) for 10 min. The washed cells were seen under the fluorescent microscope (OLYMPUS BX53, Japan).

2.15. Measures of plasma quality

2.15.1. Coagulation assays

PT and APTT measurements were performed using the coagulometer (Diagnostica STAGO, France; Fig. 3). PT and APTT tests use venous blood of patients which were decalcified using citrate ions to stop the clotting process. The plasma was separated from the blood cells by centrifugation at 4000 rpm for 20 min. The plasmas showing evidence of clot formation and/or hemolysis were discarded. The PT test was done by adding thromboplastin, to the patient's plasma that converts prothrombin to thrombin. After incubation of the mixtures in a water bath (37 °C) for one minute, the calcium chloride ($CaCl_2$) was added to the mixtures to neutralize the sodium citrate and allow clotting to start. The PT test is timed from the addition of the $CaCl_2$ until the plasma clots. This time is called PT. The PT within the 10−15 s range shows that the patient has normal amounts of the clotting factors. In the APTT test calcium, kaolin, and cephalin were added to the plasma to start the intrinsic pathway of the coagulation cascade. Kaolin serves to activate the contact-dependent Factor XII and cephalin substitutes for platelet phospholipids. The APTT is the time it takes for clot formation. Normally, it takes within 22−38 s.

2.15.2. Determination of total protein

Total plasma protein content was measured as described previously by the method of Bradford [33]. Briefly, Coomassie Brilliant Blue G-250 (Sigma-Aldrich, Steinheim, Germany) was dissolved in 95 % ethanol (100 mg/50 mL). Then, 1 mL of 85 % H_3PO_4 was added under stirring, before distilled water was added to a total volume of 10 mL. The resulting solution was filtered through a filter paper and kept at 4 °C. Standard concentrations of bovine serum albumin (BSA) (Sigma-Aldrich, Steinheim, Germany) was prepared with 0.15 M NaCl to final concentrations of 0 (blank = No protein), 25, 50, 100, and 200 μg/mL. Also, serial dilutions of the samples were prepared. 10 μL of each BSA concentrations was added to the separate well of the 96-well microplate. 50 μL of Bradford solution was added to each well and mixed gently. After 5 min the microplate was read at 595 nm wavelength. The absorbance of the standards was plotted against their concentration. The concentrations of the samples were calculated using the standard curve of BSA.

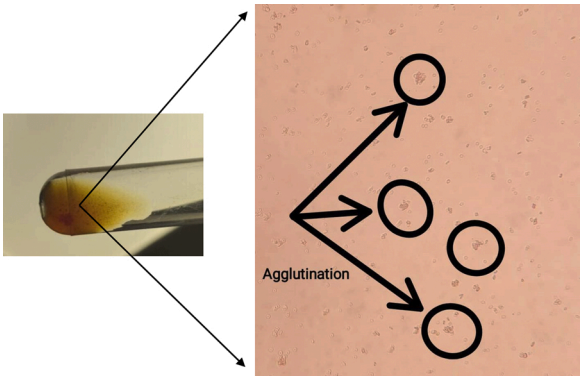

Fig. 3. Semi-auto coagulation analyzer (coagulometer) used to test the coagulation factors (PT and APTT).

2.15.3. Titration procedure

Anti-A and/or anti-B antibodies measurements were performed using a titration procedure as described previously [31]. Two-fold diluted patient's plasma was incubated in plastic tubes at room temperature with a 5% suspension of red blood cells (RBC) (A and B). Thereafter, the samples were centrifuged at 3000 rpm for 15 s to determine the highest titer where the RBC remained agglutinated after gentle shaking (Fig. 4).

2.16. Statistical assessment

Data were entered into the Statistical Package for Social Sciences (SPSS) version 23 and analyzed using one-way analysis of variance (ANOVA). The results were reported as mean ± standard deviation (SD) and P-values <0.05 were considered significant.

3. Results

3.1. Synthesized Cur@PLGA-NPs as the photosensitizing agent

The size and morphology of Cur@PLGA-NPs were investigated by SEM analysis and the ImageJ program. As can be seen in Fig. 5a, the spherical morphology is dominant. The distribution of particles is acceptable visually. To examine the particle size distribution quantitatively, about 300 particles were chosen randomly and the size of them was measured. The TEM test was used to evaluate the dispersion of Cur in the polymeric particles to demonstrate the structure of the core-shell (Fig. 5b). The dark spots in Fig. 4b represent the Cur. According to the results, the EE and LC percentage of the Cur in Cur@PLGA-NPs were 87.6 ± 3.25 % and 8.42 ± 0.23 %, respectively.

The FTIR spectra of the neat Cur, neat PLGA, and core-shell nanoparticles are shown in Fig. 5c. The board characteristic peak at ~3480 cm^{-1} was corresponding to O—H vibration of the phenol, in the Cur spectrum. The peak at ~1628 cm^{-1} was referred to as the carbonyl group. In addition, the peaks at 2963, 1430, and ~1376 cm^{-1} are associated with the C–H stretching of methyl groups. The peaks at ~1400−1500 cm^{-1} corresponded to the –C-O elongation of the

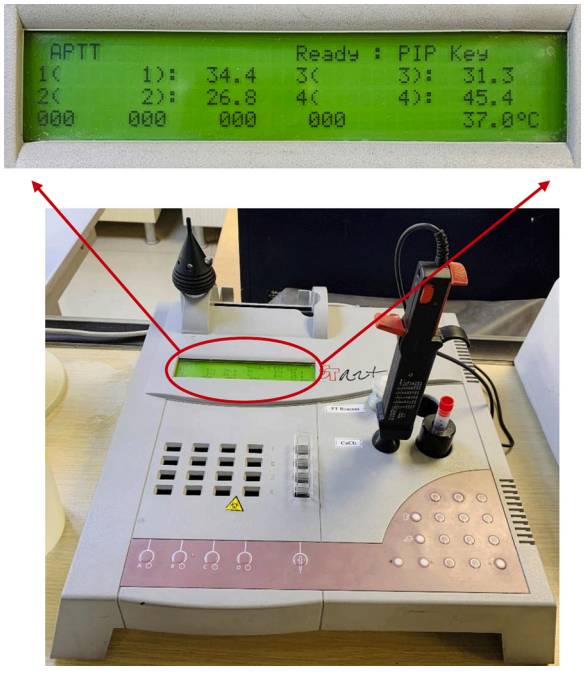

Fig. 4. Anti-A and/or anti-B antibodies measurements were performed using the titration procedure where the RBC remained agglutinated after gentle shaking.

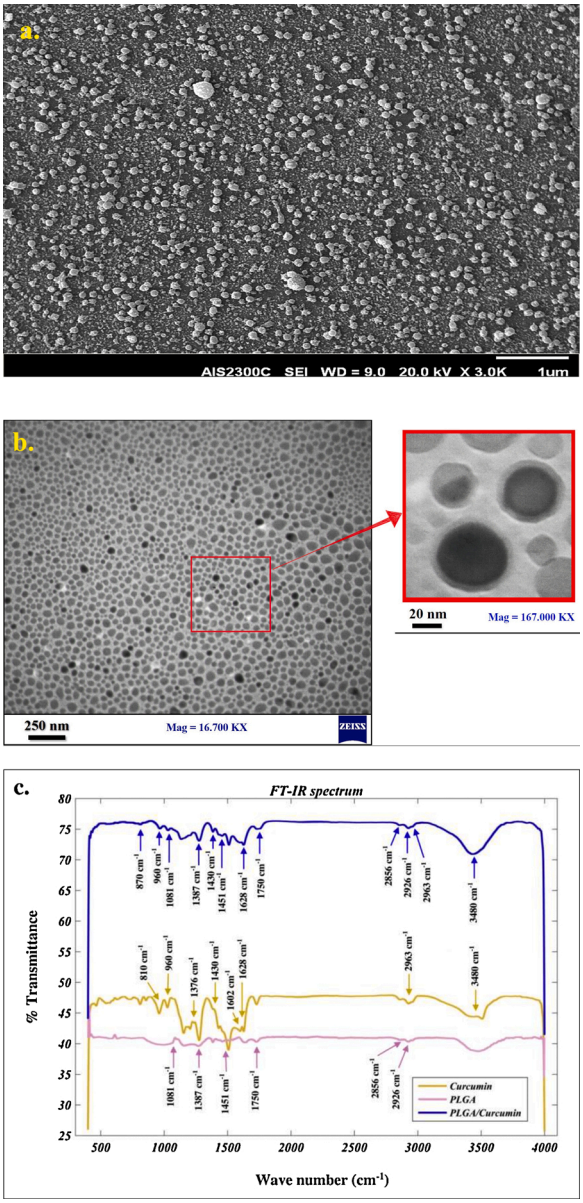

Fig. 5. Characterization of the synthesized Cur@PLGA-NLs; a) SEM image of Cur@PLGA-NLs (scale bar represents 1 μm), b) TEM image of Cur@PLGA-NLs at different magnification, Left image with less magnification (scale bar represents 250 nm), right with more magnification that shows the core-shell structure well (scale bar represents 20 nm), c) FT-IR spectra of PLGA (pink), Cur (yellow), Cur@PLGA-NLs (blue).

hydroxyl group. The CH— bending of the alkene groups has represented the peaks in the range of 700−900 cm^{-1} [34,35]. Furthermore, there is another peak at 1602 cm^{-1} that confirms the presence of aromatic rings [35].

The peaks of the mentioned polymer are located between 2850−3000 cm^{-1} and 1451 cm^{-1} which belong to the C–H of the methyl group. The C═O stretching has been characterized by a peak at ~1750 cm^{-1} [36]. Another peak for biopolymer spectra is located at 1081 cm^{-1}that signifies the presence of C—O in PLGA and the C−CH3 vibrations are depicted by the shoulder. The peaks at ~870 and 1387 cm^{-1} can be related to O—H vibrations [36,37]. The FTIR spectra of Cur@PLGA-NPs indicated that all the peaks are present and the process seems to be the summation of the PLGA and Cur spectra, an indication of the intact molecular structure of primary components after blending and electrospraying. In brief, the electrospray method does not change the material's nature.

3.2. UV–vis spectra of Cur@PLGA-NPs

The UV–vis spectrum of Cur@PLGA-NPs aqueous solution is presented in Fig. 6. As shown, the absorption spectrum of Cur@PLGA-NPs is a broadband with a maximum absorbance peak at a wavelength ~425 nm, which could be assigned to low energy π–π* excitation of the Cur, as reported in Kim et al. [38]. This peak is typical for Cur.

3.3. Physical stability of Cur@PLGA-NPs during storage

Cur@PLGA-NPs stability was measured by particle size over 30 days at 4 °C and 37 °C, which showed no significant variation between day 0 and day 30 ($P > 0.05$; Fig. 7). No significant changes were achieved in the polydispersity index ($P > 0.05$) and zeta potential ($P > 0.05$) during 30 days at 4 °C and 37 °C, indicating that there was no aggregation.

3.4. Confirmation of the presence of SARS-CoV-2 by detection of ORF1ab gene

The amplification of *ORF1ab* gene in the synthesized cDNA template was confirmed the presence of SARS-CoV-2 (84.3 %). A 2% gel agarose and an amplification curve of samples for SARS-CoV-2 detection based on the *ORF1ab* gene were shown in Figs. 8a and b.

3.5. Efficacy of photosensitizer, blue laser light, and aPDT on Vero cell lines

To determine the maximum sub-cytotoxic effect of aPDT for treatment of plasma containing SARS-CoV-2, the Vero cell cytotoxicity of different concentrations of Cur@PLGA-NPs alone, different energy doses of blue laser alone, and aPDT with several blue laser energy doses (104.5, 313.7, and 522.8 J/cm^2) in combination with the different Cur@PLGA-NPs concentrations (3, 5, 7, 10, and 15 %) were investigated. Different concentrations of Cur@PLGA-NPs (3, 5, 7, and 10 %) lonely had no effect on viable cells (1.5, 4.0, 5.8, 6.8, and 23.4 % reduction, respectively); it was nearly the same as the untreated control group. Increasing Cur@PLGA-NPs concentration further to 15 % caused a statistically significant cytotoxic effect (23.4 %) compared to the untreated control group ($P < 0.05$) and it was not the desired effect of Cur@PLGA-NPs (Fig. 9a).

On the other hand, laser energy doses of 104.5, 313.7, and 522.8 J/cm^2 caused around 2.8, 4.7, and 10.9 % reduction in the viable cell count when applied alone, respectively (Fig. 9b). These energy doses alone did not cause any significant change in cell number ($P > 0.05$).

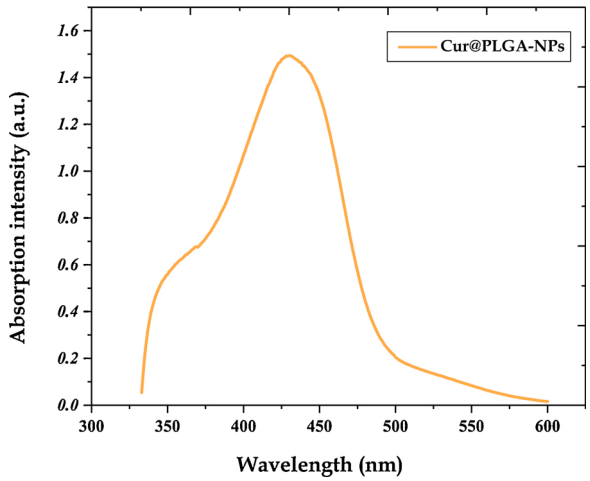

Fig. 6. UV–vis absorption spectra of Cur@PLGA-NLs.

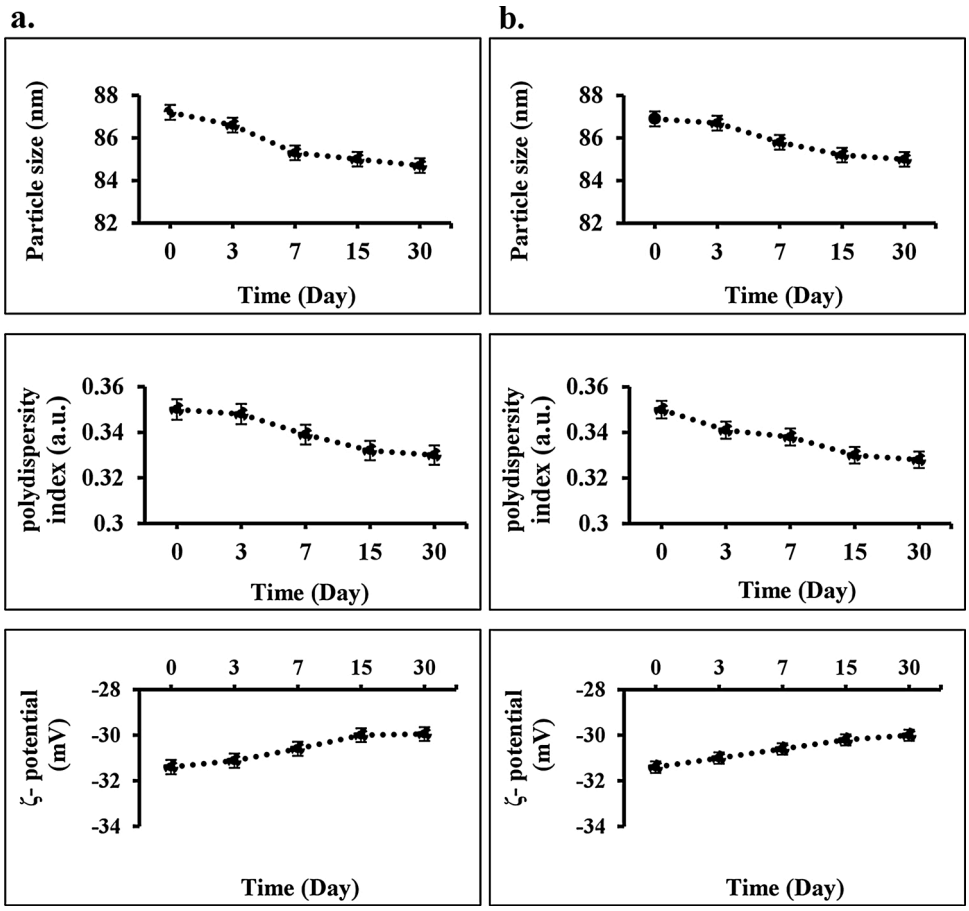

Fig. 7. Measurement of physical stability of Cur@PLGA-NPs during storage using particle size, polydispersity index, and zeta potential of Cur@PLGA-NLs in different conditions; a) at 4 °C, b) at 37 °C.

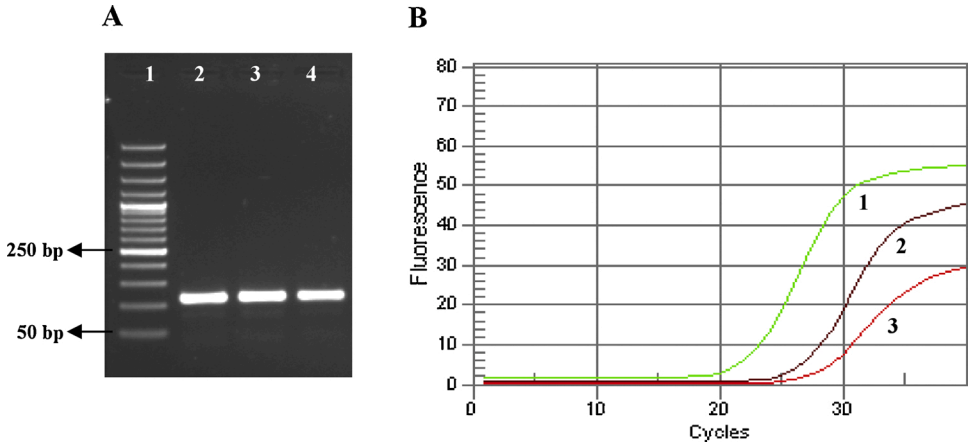

Fig. 8. Confirmation of the presence of SARS-CoV-2 by detection of *ORF1ab* gene: A) The cDNA template synthesized from *ORF1ab* on the 2% gel agarose: 1. Ladder 50 bp, 2. Control positive (108 bp), 3 and 4. Two positive samples (108 bp). B) The amplification curves of positive samples: 1. Control positive, 2 and 3. Two positive samples.

104.5 J/cm^2 of light with 3, 5, 7, and 10 % of Cur@PLGA-NPs resulted in the statistically non-significant amount of cell reduction in all of the Cur@PLGA-NPs doses tested (5.4 %, 9.6 %, 12.3 %, and 14.7 % respectively; all $P > 0.05$). When all of the Cur@PLGA-NPs doses tested (3, 5, 7, and 10 %, respectively) were used with 313.7 J/cm^2 of energy dose, there was almost no significant change in the number of viable cells compared to the untreated control group (8.1 %, 11.7 %, 15.9 %, and 17.1 %, respectively; all $P > 0.05$; Fig. 9c). An energy dose of 522.8 J/cm^2 did not cause any significant change in the viable cell count when applied with 3, 5, 7, and 10 % of Cur@PLGA-NPs (10.3 %, 14.2 %, 17.0 %, and 19.9 % respectively; $P > 0.05$). Towards the end of this Cur@PLGA-NPs concentration range, the desired effect of aPDT following treatment of cell culture with maximum dosed of blue laser light (522.8 J/cm^2) and 10 % of Cur@PLGA-NPs achieved by a non-significant decrease in the number of viable cells. The sub-cytotoxic effect of aPDT (10 % wt. Cur@PLGA-NPs plus 522.8 J/cm^2 dose of

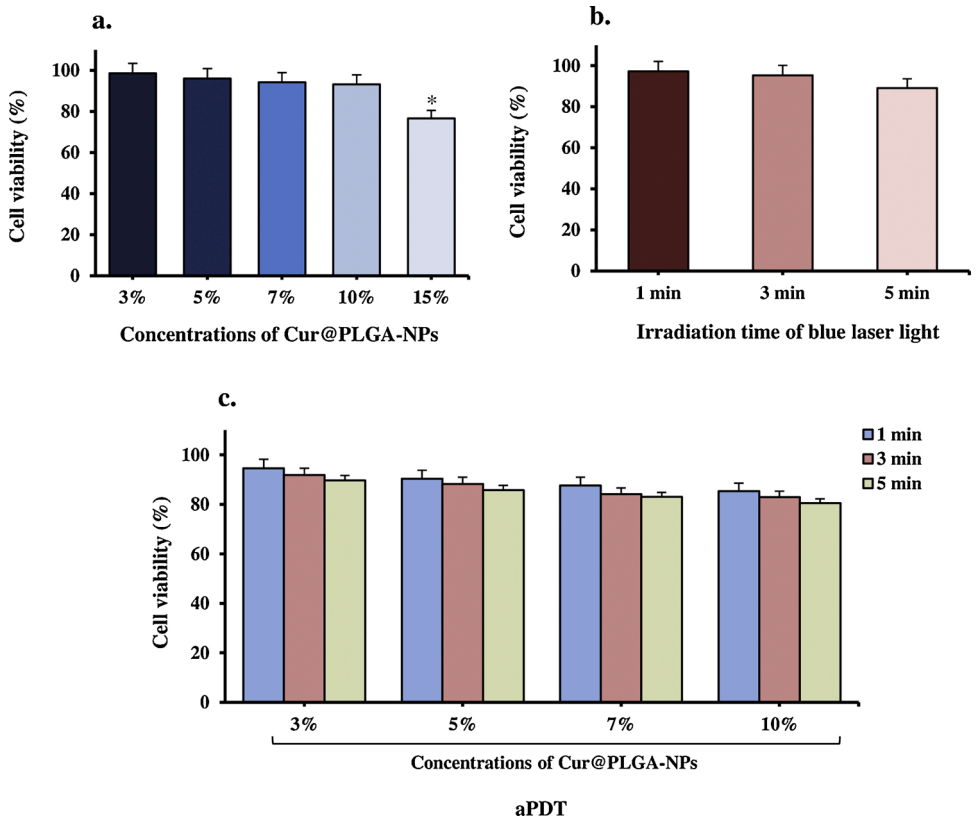

Fig. 9. Determination of the Vero cells viability by MTT assay at 540 nm; I) Treated Vero cells with different concentrations of Cur@PLGA-NLs, II) Treated Vero cells with different irradiation times of blue laser light, and III) Treated Vero cells with aPDT using 10 % wt. Cur@PLGA-NPs plus blue laser light at an energy density of 522.8 J/cm^2.

blue laser light) was used for the treatment of plasma containing SARS-CoV-2.

3.6. Determination of cell cytotoxicity of Vero cells with treated plasma containing SARS-CoV-2

The Vero cells were infected with treated plasma by aPDT at the non-cytotoxic highest concentration of Cur@PLGA-NPs (10 % wt.) and the highest energy density of the blue laser light (522.8 J/cm^2). The results of the viral cytotoxicity using the MTT assay were presented in Fig. 10.

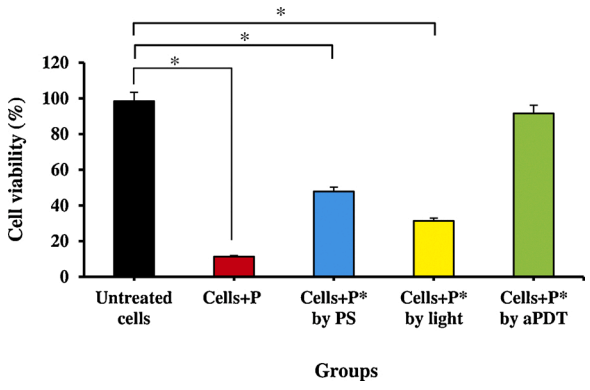

Fig. 10. Determination of the cell cytotoxicity of Vero cells with treated plasma containing SARS-CoV-2 by MTT assay at 540 nm; P: Untreated plasma containing SARS-CoV-2, P*: Treated plasma containing SARS-CoV-2, PS: Photosensitizer (10 % wt. Cur@PLGA-NPs), aPDT: 10 % wt. Cur@PLGA-NPs plus blue laser light at an energy density of 522.8 J/cm^2. Significant differences according to the control.
* $P < 0.05$.

Based on the results of these experiments, it was found that there was significant cell reduction in treated Vero cells with treated plasma containing SARS-CoV-2 using 10 % wt. Cur@PLGA-NPs, as well as, blue laser light at an energy density of 522.8 J/cm^2 alone by 52.2 % and 68.7 %, respectively. Furthermore, treated plasma containing SARS-CoV-2 with aPDT (10 % wt. Cur@PLGA-NPs plus blue laser light at 522.8 J/cm^2) did not cytotoxic effect on the Vero cell line (Fig. 10).

3.7. Assessment of the apoptotic effects in treated Vero cells with treated plasma containing SARS-CoV-2

To explore the effect of photosensitizer, blue laser light, and aPDT on Vero cell apoptosis, flow cytometry and fluorescent staining assays were performed in our investigation. Flow cytometry analysis demonstrated that exposure to plasma containing SARS-CoV-2 had a marked apoptotic effect (86.1 %) on Vero cells, with a complete decline in cell culture viability (Fig. 11a). Consistent with this observation in Figs. 11c and d, the results of flow cytometric analysis indicated a significant increase in the apoptotic population of treated Vero cells with Cur@PLGA-NPs and laser light alone (33.7 % and 49.3 %, respectively) compared with a control group (Untreated Vero cells). On the other hand, unlike infected Vero cells with plasma containing SARS-CoV-2 (Fig. 11b), considerable apoptotic effects were not observed in treated Vero cells with treated plasma containing SARS-CoV-2 by aPDT (Fig. 11e).

In the fluorescent staining analysis, no significant apoptosis was observed in the Vero cells in the control groups (Fig. 12a). Apoptotic Vero cells, marked by AO/EB staining (nuclear yellow-green and orange color), were seen in treated Vero cells with plasma containing SARS-CoV-2 (Fig. 12b). The apoptotic effects of treated plasma containing SARS-CoV-2 with 10 % wt. Cur@PLGA-NPs on Vero cells were similar to those treated with blue laser light alone (Fig. 12c and d). As shown in Fig. 12e, no significant increase in the apoptotic population of treated

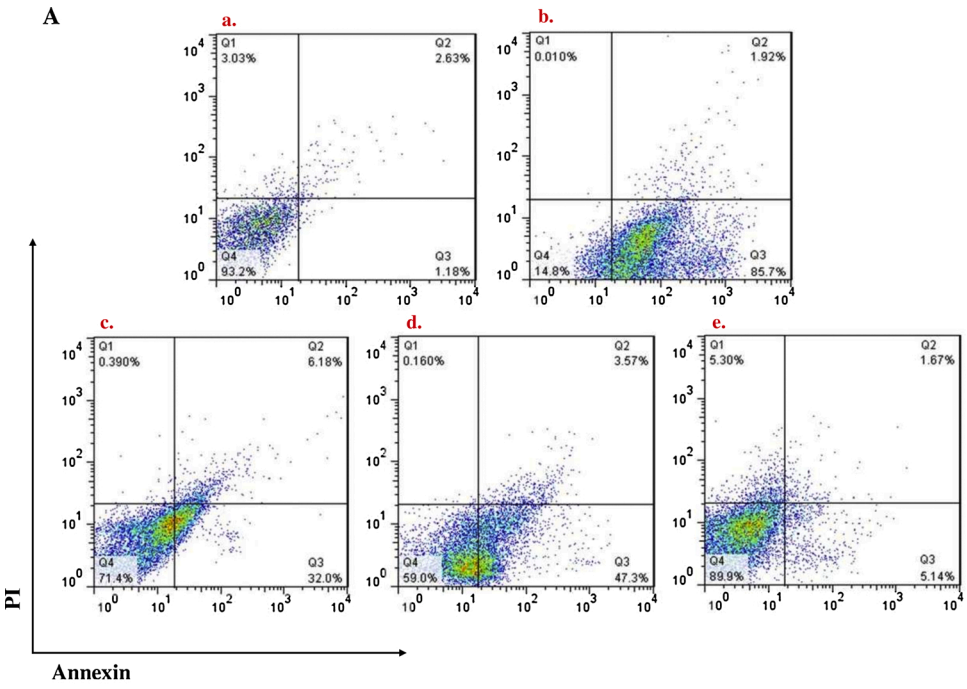

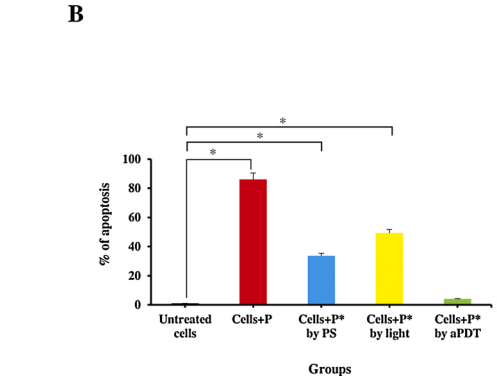

Fig. 11. Determination of the apoptotic effects in treated Vero cells with treated plasma containing SARS-CoV-2; A) The apoptotic ratio was assessed by flow cytometry with Annexin V staining in Vero cells: a. Untreated Vero cells (as a control group), b. Treated Vero cells with untreated plasma containing SARS-CoV-2, c) Treated Vero cells with treated plasma containing SARS-CoV-2 using 10 % wt. Cur@PLGA-NPs, d) Treated Vero cells with treated plasma containing SARS-CoV-2 using blue laser light at an energy density of 522.8 J/cm^2, e) Treated Vero cells with treated plasma containing SARS-CoV-2 using aPDT with 10 % wt. Cur@PLGA-NPs plus blue laser light at an energy density of 522.8 J/cm^2. B) Percent of cell viability at 540 nm. P: Untreated plasma containing SARS-CoV-2, P*: Treated plasma containing SARS-CoV-2. PS: Photosensitizer (10 % wt. Cur@PLGA-NPs). Significant differences according to the control, * $P < 0.05$.

Vero cells with treated plasma containing SARS-CoV-2 by aPDT.

3.8. Determination of PDT induced adverse effects on plasma quality

The results of total plasma protein content, basic coagulation tests (PT and APTT), and anti-A and/or anti-B antibodies titers were showed in Table 1. Total plasma protein content, PT, APTT, and anti-A and/or anti-B antibodies titers showed no significant changes ($P > 0.05$ for all comparisons) in treated plasma as compared to untreated plasma.

4. Discussion

Many diagnostic tests for COVID-19 are available including RT-PCR, loop-mediated isothermal amplification (LAMP), lateral flow, and enzyme-linked immunosorbent assay (ELISA) [39,40]. Currently, RT-PCR assay, as a method for detecting the presence of specific genetic material even in low copy numbers, is used for detection of SARS-CoV-2 in the nasopharyngeal swab, sputum, blood, and stool samples of patients [41]. Herein, the positive test results were determined based on the Ct-value less than 37 according to the IVDC.

Recently, aPDT has emerged as a promising therapeutic approach for the treatment of different diseases. The antiviral activities of aPDT are of interest as an alternative tool in antiviral treatments [24–27]. Another aspect of photodynamic action of aPDT against viruses, currently attracting considerable interest, is no resistance to aPDT was reported [22]. Nucleic acids (DNA or RNA), virus proteins, and viral lipids are three principal molecular targets for aPDT. During aPDT, the photosensitizing agent can cross the outer cover of viruses and intercalate into their DNA/RNA [42]. Antiviral activity of produced ROS under blue laser light irradiation has been shown [8].

Although there is no evidence specifically investigating the effect of aPDT on viral lipids and/or proteins, there are investigations about the effect of ROS on viral lipids [43–45]. Since there are viral lipids in the envelope of the SARS-CoV-2, it should probably be sensitive to the effects of aPDT. As an antiviral agent, Cur has been reported to play a potent role in the regulation of proliferation and apoptosis in various types of viral cells. The results of Maiti et al. [46] study suggested that Cur has potent inhibitory properties of growth for glioblastoma multiforme cells and can rapidly kill the malignant glioma cells *via* DNA fragmentation. As well as, Cur induced cell death due to excess production of ROS.

In this study, PLGA was used to overcome the poor bioavailability of Cur due to its low water-solubility. Electrical conductivity, polymer concentration, solvent system, and electrospinning process parameters affect the size and final morphology of obtained particles. So, these parameters were determined with high accuracy for achieving smaller

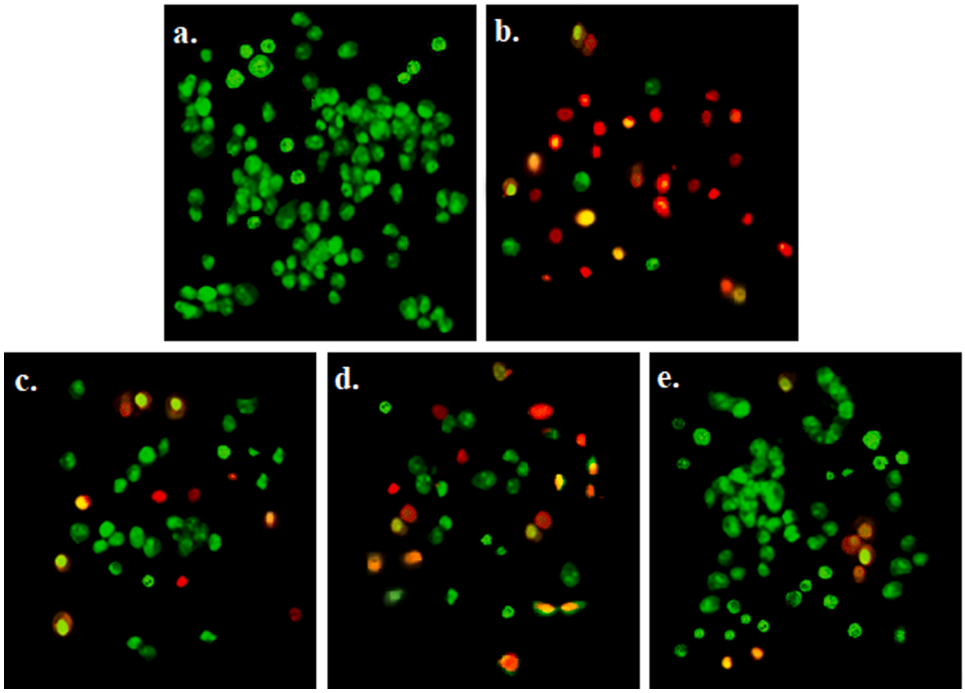

Fig. 12. Determination of the apoptotic effects in exposed Vero cells by acridine orange /ethidium bromide fluorescent staining under the fluorescent microscope (OLYMPUS BX53, Japan; objective magnification 10x; Scale bars=100 μm): a) Untreated Vero cells, as a control group, revealing green nuclear staining, b) Exposed Vero cell culture with untreated plasma containing SARS-CoV-2 showing a large number of apoptotic cells which had orange and red nuclear fluorescence emission, c) Exposed Vero cell culture with treated plasma containing SARS-CoV-2 using 10 % wt. Cur@PLGA-NPs, indicating decrease in cells with orange-red nuclear staining in comparison to exposed Vero cell culture with untreated plasma containing SARS-CoV-2, d) Exposed Vero cell culture with treated plasma containing SARS-CoV-2 using blue laser light (522.8 J/cm^2) representing increase the number of apoptotic cells more than exposed Vero cells with treated plasma containing SARS-CoV-2 using 10 % wt. Cur@PLGA-NPs and less than exposed Vero cells with untreated plasma containing SARS-CoV-2, e) Exposed Vero cells with treated plasma containing SARS-CoV-2 using aPDT with 10 % wt. Cur@PLGA-NPs plus blue laser light (522.8 J/cm^2) demonstrating a significant reduction in the number of apoptotic cells in comparison to exposed Vero cells with untreated plasma containing SARS-CoV-2.

Table 1
The total plasma protein content, PT, APTT, and anti-A and/or anti-B antibodies titers results before and after aPDT treatment.[#]

Analytes	Reference range	Before treatment	After treatment	*p*-value*
Total plasma protein (g/L)	≥ 50	68.5 ± 4.3	63.1 ± 5.7	<0.001
PT	10–15	12.8 ± 1.7	13.9 ± 1.4	<0.001
APTT	22–38	31.3 ± 3.9	33.4 ± 5.4	<0.001
anti-A min : max 16 : 512				
<128	–	92.6 %	92.6 %	<0.001
<32	–	11.1 %	14.8 %	<0.001
anti-B min : max 16 : 1024				
<128	–	89.9 %	92.9 %	<0.001
<32	–	18.5 %	18.5 %	<0.001

[#] Data of PT, APTT, and Total plasma protein are presented as mean ± SD.

particles [21].

As FTIR results showed, the addition of Cur to the system did not change the nature of that since the spectra of the nanoparticles indicated the summation of the PLGA and Cur spectra.

Herein, the Vero cell was used as an appropriate cell line for COVID-19 propagation. To confirm the potential role of aPDT in Vero cell growth, MTT assay was performed to assess the cell viability after treatment with Cur@PLGA-NPs over a wide range of concentrations and different irradiation times of blue laser. Regarding the collected data, there were no significant changes in the viability of Vero cells after treatment with different concentrations of Cur@PLGA-NPs, irradiation times of blue laser light, as well as, aPDT.

The most commonly used clinical application of the aPDT is currently the field of viral decontamination of blood products [24–27]. Recently, the inactivation of various viruses such as SARS-CoV-2 and MERS-CoV in plasma products using aPDT was investigated. Jin et al. [24] conducted aPDT with methylene blue (MB) as a photosensitizer that could be effective against SARS-CoV-2 in plasma without any side effects. According to the results, different concentrations of MB (1, 2, and 4 Mm) under the wavelength of 630 nm light for 2 min could completely inactivate the virus and the viral titer of SARS-CoV-2 decreased to 4.5 $\log_{10}$ median tissue culture infectious dose (TCID50)/mL. As commented by Eickmann et al. [25,26], MB plus visible light at the light doses as low as 30 J/cm^2, is capable to reduce SARS-CoV and MERS-Cov more than 3.1 and 3.3 $\log_{10}$ $TCID_{50}$/mL in plasma, respectively. In another study by Keil et al. [27], the inactivation of the MERS-CoV was evaluated using a riboflavin-based and ultraviolet light-based photochemical treatment in plasma products. The mean reductions in the log titer of MERS-CoV for the pooled and individual donor plasma were ≥ 4.07 and ≥ 4.42, respectively.

According to the collected data from this study, there was a considerable cell degradation in the treated Vero cells with treated plasma containing SARS-CoV-2 using Cur@PLGA-NPs and blue laser light alone. In addition, cell degradation was not only observed during aPDT, but also the viability of treated Vero cells with treated plasma containing SARS-CoV-2 was similar to the untreated Vero cell (as a control group). Similar to the previous studies, aPDT could significantly reduce the titer of SARS-CoV-2 in plasma without damaging the Vero cells [25–27]. There were no significant changes in the anticoagulation factors (PT and APTT), total plasma protein content, and anti-A and/or anti-B antibodies titers between before and after aPDT treatment, thus indicating no adverse effects on plasma quality in aPDT-exposed plasma which could induce the inactivation of SARS-CoV-2 contaminants.

Results suggested that a higher concentration of Cur@PLGA-NPs and time of light irradiation-induced apoptotic activity by annexin-V/PI staining in the treated Vero cells with treated plasma containing SARS-CoV-2. Also, the apoptotic activities of Cur@PLGA-NPs and blue laser were significantly higher than aPDT and control groups. Based on the data obtained, it could be concluded that aPDT exhibited *in vitro* anti−COVID-19 activities without induction of apoptosis and destruction of Vero cells.

5. Conclusion

Our data support that aPDT (10 % wt. Cur@PLGA-NPs in combination with blue laser light at 522.8 J/cm^2) exhibited *in vitro* anti−COVID-19 activity without the cytotoxic effects in Vero cells culture by a treated plasma containing SARS−COV-2. However, further *in vivo* animal and clinical trial studies are needed to confirm the effect of aPDT (Cur@PLGA-NPs in combination with blue laser light) on plasma clearance of SARS-CoV-2. Our study also clearly revealed that the quality of aPDT-exposed plasma is not significantly influenced by aPDT based on Cur@PLGA-NPs.

Statement of ethics

This study was approved by the Ethics Committee of Tehran University, Faculty of Medicine (IR.TUMS.VCR.REC.1399.490).

Declaration of Competing Interest

The authors declare that there is no conflict of interests regarding the publication of this paper.

Acknowledgement

This research has been supported by Tehran University of Medical Sciences & Health Services grant No. 99-2-101-48394.

References

[1] X.W. Xu, X.X. Wu, X.G. Jiang, K.J. Xu, L.J. Ying, C.L. Ma, et al., Clinical findings in a group of patients infected with the 2019 novel coronavirus (SARS-Cov-2) outside of Wuhan, China: retrospective case series, bmj 19 (2020) 368–372.
[2] U. Pradesh, P.D. Upadhayay, P.C. Vigyan, Coronavirus infection in equines: a review, Asian J. Anim. Vet. Adv. 9 (2014) 164–176.
[3] C. Wang, X. Zheng, W. Gai, Y. Zhao, H. Wang, H. Wang, et al., MERS-CoV virus-like particles produced in insect cells induce specific humoural and cellular immunity in rhesus macaques, Oncotarget. 8 (2017) 12686–12694.
[4] A. ul Rehman, S.A. Qureshi, The role of primary and secondary bio-molecules in optical diagnosis of pandemic COVID-19 outbreak, Photodiagnosis Photodyn. Ther. 31 (2010) 1–2.
[5] K. Takayama, In vitro and animal models for SARS-CoV-2 research, Trends Pharmacol. Sci. 41 (2020) 513–517.
[6] J. Kaiser-Guignard, G. Canellini, N. Lion, M. Abonnenc, J.C. Osselaer, J.D. Tissot, The clinical and biological impact of new pathogen inactivation technologies on platelet concentrates, Blood 28 (2014) 235–241.
[7] G. Jori, O. Coppellotti, Inactivation of pathogenic microorganisms by photodynamic techniques: mechanistic aspects and perspective applications, Current. Med. Chemis. Anti-Infec. Agen. 6 (2007) 119–131.
[8] Y. Seo, K. Park, Y. Hong, E.S. Lee, S.S. Kim, Y.T. Jung, et al., Reactive-oxygen-species-mediated mechanism for photoinduced antibacterial and antiviral activities of Ag3PO4, Anal. Sci. Technol. 11 (2020) 1–6.
[9] T.N. Demidova, M.R. Hamblin, Photodynamic therapy targeted to pathogens, Int. J. Immunopathol. Pharmacol. 17 (2004) 245–254.
[10] V.V. Zarubaev, I.M. Belousova, O.I. Kiselev, L.B. Piotrovsky, P.M. Anfimov, T. C. Krisko, et al., Photodynamic inactivation of influenza virus with fullerene C60 suspension in allantoic fluid, Photodiagnosis Photodyn. Ther. 4 (2007) 31–35.
[11] M.J. Shikowitz, A.L. Abramson, K. Freeman, B.M. Steinberg, M. Nouri, Efficacy of DHE photodynamic therapy for respiratory papillomatosis: immediate and long-term results, Laryngoscope. 108 (1998) 962–967.
[12] A.L. Abramson, M.J. Shikowitz, V.M. Mullooly, B.M. Steinberg, C.A. Amella, H. R. Rothstein, Clinical effects of photodynamic therapy on recurrent laryngeal papillomas, Arch. Otolaryngol. Head Neck Surg. 118 (1992) 25–29.
[13] A. Wiehe, J.M. O'Brien, M.O. Senge, Trends and targets in antiviral phototherapy, Photochem. Photobiol. Sci. 18 (2019) 2565–2612.
[14] C.M. Allen, J.M. Weber, J.E. van Lier, Sulfophthalocyanines for photodynamic inactivation of viruses in blood products: effect of structural modifications, Photochem. Photobiol. 62 (1995) 184–189.
[15] V.H. Panhóca, F.L. Esteban Florez, T.Q. Corrêa, F.R. Paolillo, C.W. de Souza, V. S. Bagnato, Oral decontamination of orthodontic patients using photodynamic therapy mediated by blue-light irradiation and curcumin associated with sodium dodecyl sulfate, Photomed. Laser Surg. 34 (2016) 411–417.
[16] P. Anand, A.B. Kunnumakkara, R.A. Newman, B.B. Aggarwal, Bioavailability of curcumin: problems and promises, Mol. Pharm. 4 (2007) 807–818.
[17] X. Xie, Q. Tao, Y. Zou, F. Zhang, M. Guo, Y. Wang, et al., PLGA nanoparticles improve the oral bioavailability of curcumin in rats: characterizations and mechanisms, J. Agric. Food. Chem. 59 (2011) 9280–9289.
[18] M. Gao, X. Long, J. Du, M. Teng, W. Zhang, Y. Wang, et al., Enhanced curcumin solubility and antibacterial activity by encapsulation in PLGA oily core nanocapsules, Food Funct. 11 (2020) 448–455.
[19] M.Y. Hsu, Y.T. Huang, C.J. Weng, C.M. Chen, Y.F. Su, S.Y. Chu, et al., Preparation and in vitro/in vivo evaluation of doxorubicin-loaded poly [lactic-co-glycol acid] microspheres using electrospray method for sustained drug delivery and potential intratumoral injection, Colloids Surf. B Biointerfaces 190 (2020) 1–7.
[20] A. Haslberger, U. Jacob, B. Hippe, H. Karlic, Mechanisms of selected functional foods against viral infections with a view on COVID-19: mini review, Funct. Food. Health. dis. 10 (2020) 195–209.
[21] H. Ahmadi, V. Haddadi-Asl, H.A. Ghafari, R. Ghorbanzadeh, Y. Mazlum, A. Bahador, Shear bond strength, adhesive remnant index, and anti-biofilm effects of a photoexcited modified orthodontic adhesive containing curcumin doped poly lactic-co-glycolic acid nanoparticles: an ex-vivo biofilm model of S. Mutans on the enamel slab bonded brackets, Photodiagnosis Photodyn. Ther. 30 (2020) 1–7.
[22] M.R. Hamblin, T. Hasan, Photodynamic therapy: a new antimicrobial approach to infectious disease? Photochem. Photobiol. Sci. 3 (2004) 436–450.
[23] M. Wainwright, Local treatment of viral disease using photodynamic therapy, Int. J. Antimicrob. Agents 21 (2003) 510–520.
[24] C. Jin, B. Yu, J. Zhang, H. Wu, X. Zhou, H. Yao, et al., Methylene blue photochemical treatment as a reliable SARS-CoV-2 plasma virus inactivation method for blood safety and convalescent plasma therapy for the COVID-19 outbreak, Res. Square. 1 (2020) 1–15.
[25] M. Eickmann, U. Gravemann, W. Handke, F. Tolksdorf, S. Reichenberg, T. H. Müller, et al., Inactivation of three emerging viruses - severe acute respiratory syndrome coronavirus, Crimean-Congo haemorrhagic fever virus and Nipah virus – in platelet concentrates by ultraviolet C light and in plasma by methylene blue plus visible light, Vox Sang. (2020), https://doi.org/10.1111/vox.12888.
[26] M. Eickmann, U. Gravemann, W. Handke, F. Tolksdorf, S. Reichenberg, T. H. Müller, et al., Inactivation of Ebola virus and Middle East respiratory syndrome coronavirus in platelet concentrates and plasma by ultraviolet C light and methylene blue plus visible light, respectively, Transfusion. 58 (2018) 2202–2207.
[27] S.D. Kei, R. Bowen, S. Marschner, Inactivation of Middle East respiratory syndrome coronavirus (MERS-CoV) in plasma products using a riboflavin-based and ultraviolet light-based photochemical treatment, Transfusion. 56 (2016) 2948–2952.
[28] S. Ramirez-Arcos, D.C. Marks, J.P. Acker, W.P. Sheffield, Quality and safety of blood products, J. Blood Transfus. 2016 (2016) 2482157–2482162.
[29] Z. Wang, H. Liu, M. Dou, X. Du, J. Hu, N. Su, et al., The quality changes in fresh frozen plasma of the blood donors at high altitude, PLoS One 12 (2017), e0176390.
[30] J.D. Folds, J.L. Schmitz, Clinical and laboratory assessment of immunity, J. Allergy Clin. Immunol. 111 (2003) 702–711.
[31] G. Denomme, Titers of ABO antibodies in group O blood donors: patient safety and blood product supply remain a challenge, Rev. Bras. Hematol. Hemoter. 33 (2011) 250–251.
[32] M. Pourhajibagher, A. Partoazar, M. Alaeddini, S. Etemad-Moghadam, A. Bahador, Photodisinfection effects of silver sulfadiazine nanoliposomes doped-curcumin on Acinetobacter baumannii: a mouse model, Nanomedicine. 15 (2020) 437–452.
[33] M.M. Bradford, A rapid and sensitive method for the quantitation of microgram quantities of protein utilizing the principle of protein-dye binding, Anal. Biochem. 72 (1976) 248–254.
[34] C. Yucel, V. Quagliariello, R.V. Iaffaioli, G. Ferrari, F. Donsì, Submicron complex lipid carriers for curcumin delivery to intestinal epithelial cells: effect of different emulsifiers on bioaccessibility and cell uptake, Int. J. Pharm. 494 (2015) 357–369.
[35] T. Jiaju, W. Jin, P. Changjiang, W. Yajun, H. Nan, Anticoagulation and drug release behavior of Curcumin-Loaded PLGA films, Key Eng. Mater. 342 (2007) 481–484.
[36] M.A. Akl, A. Kartal-Hodzic, T. Oksanen, H.R. Ismael, M.M. Afouna, M. Yliperttula, et al., Factorial design formulation optimization and in vitro characterization of curcumin-loaded PLGA nanoparticles for colon delivery, J. Drug Deliv. Sci. Technol. 32 (2016) 10–20.
[37] Z. Esmaili, S. Bayrami, F.A. Dorkoosh, H. Akbari Javar, E. Seyedjafari, S. S. Zargarian, et al., Development and characterization of electrosprayed nanoparticles for encapsulation of C urcumin, J. Biomed. Mater. Res. A. 106 (2018) 285–292.
[38] H.J. Kim, D.J. Kim, S.N. Karthick, K.V. Hemalatha, C.J. Raj, S. Ok, et al., Curcumin dye extracted from Curcuma longa L. Used as sensitizers for efficient dye-sensitized solar cells, Int. J. Electrochem. Sci. 8 (2013) 8320–8325.
[39] L.J. Carter, L.V. Garner, J.W. Smoot, Y. Li, Q. Zhou, C.J. Saveson, et al., Assay techniques and test development for COVID-19 diagnosis, ACS Cent. Sci. 6 (2020) 591–605.
[40] B. Udugama, P. Kadhiresan, H.N. Kozlowski, A. Malekjahani, M. Osborne, V.Y. Li, et al., Diagnosing COVID-19: the disease and tools for detection, ACS Nano 14 (2020) 3822–3835.
[41] Y. Li, L. Yao, J. Li, L. Chen, Y. Song, Z. Cai, et al., Stability issues of RT-PCR testing of SARS-CoV-2 for hospitalized patients clinically diagnosed with COVID-19, J. Med. Virol. 92 (2020) 903–908.
[42] A. Wiehe, J.M. O'Brien, M.O. Senge, Trends and targets in antiviral phototherapy, Photochem. Photobiol. Sci. 18 (2019) 2565–2612.
[43] L. Costa, M.A.F. Faustino, M.S.M.G. Neves, A. Cunha, A. Almeida, Photodynamic inactivation of mammalian viruses and bacteriophages, Viruses. 4 (2012) 1034–1074.

[44] M.S. Baptista, J. Cadet, P. Di Mascio, A.A. Ghogare, A. Greer, M.R. Hamblin, et al., Type I and Type II photosensitized oxidation reactions: guidelines and mechanistic pathways, Photochem. Photobiol. 93 (2017) 912–919.
[45] A.W. Girotti, Photosensitized oxidation of membrane lipids: reaction pathways, cytotoxic effects, and cytoprotective mechanisms, J. Photochem. Photobiol. B, Biol. 63 (2001) 103–113.
[46] P. Maiti, A. Al-Gharaibeh, N. Kolli, G.L. Dunbar, Solid lipid curcumin particles induce more DNA fragmentation and cell death in cultured human glioblastoma cells than does natural curcumin, Oxid. Med. Cell. Longev. 2017 (2017) 1–17.